

Improved stability of amorphous $InGaZnO_4$ thin-film transistors under negative bias illumination stress with the incorporation of fluorine passivation and metal shielding lines

Yuhan Feng(冯雨涵), Nannan Lv(吕楠楠), Huaisheng Wang(王槐生), Mingxiang Wang(王明湘), and Dongli Zhang(张冬利)

Citation: Chin. Phys. B, 2026, 35 (**5**): 058103. DOI: 10.1088/1674-1056/ae40da
http://cpb.iphy.ac.cn; http://iopscience.iop.org/cpb

What follows is a list of articles you may be interested in

Plastic deformation mechanism of *γ*-phase U-Mo alloy studied by molecular dynamics simulations

Chang Wang(王畅), Peng Peng(彭芃), and Wen-Sheng Lai(赖文生)
Chin. Phys. B, 2025, 34 (**1**): 018101. DOI: 10.1088/1674-1056/ad925e

Effect of external magnetic field on the instability of THz plasma waves in nanoscale graphene field-effect transistors

Liping Zhang(张丽萍), Zongyao Sun(孙宗耀), Jiani Li(李佳妮), and Junyan Su(苏俊燕)
Chin. Phys. B, 2024, 33 (**4**): 048102. DOI: 10.1088/1674-1056/ad1e66

Degradation mechanisms for a-InGaZnO thin-film transistors functioning under simultaneous DC gate and drain biases

Tianyuan Song(宋天源), Dongli Zhang(张冬利), Mingxiang Wang(王明湘), and Qi Shan(单奇)
Chin. Phys. B, 2022, 31 (**8**): 088101. DOI: 10.1088/1674-1056/ac673e

Degradation and its fast recovery in a-IGZO thin-film transistors under negative gate bias stress

Jianing Guo(郭佳宁), Dongli Zhang(张冬利), Mingxiang Wang(王明湘), and Huaisheng Wang(王槐生)
Chin. Phys. B, 2021, 30 (**11**): 118102. DOI: 10.1088/1674-1056/ac05aa

A systematic study of light dependency of persistent photoconductivity in a-InGaZnO thin-film transistors

Yalan Wang(王雅兰), Mingxiang Wang(王明湘), Dongli Zhang(张冬利), and Huaisheng Wang(王槐生)
Chin. Phys. B, 2020, 29 (**11**): 118101. DOI: 10.1088/1674-1056/abb222

Improved stability of amorphous $InGaZnO_4$ thin-film transistors under negative bias illumination stress with the incorporation of fluorine passivation and metal shielding lines

Yuhan Feng(冯雨涵), Nannan Lv(吕楠楠), Huaisheng Wang(王槐生), Mingxiang Wang(王明湘), and Dongli Zhang(张冬利)†

School of Electronic and Information Engineering, Soochow University, Suzhou 215006, *China*

(Received 16 November 2025; revised manuscript received 15 January 2026; accepted manuscript online 3 February 2026)

The instability phenomenon under negative bias illumination stress (NBIS) remains a major challenge for the application of amorphous indium gallium zinc oxide (a-IGZO) thin-film transistors (TFTs) in active-matrix displays. In this paper, we employ fluorine plasma treatment and a segmented metal cover line approach to enhance the stability of elevated metal metal-oxide (EMMO) a-IGZO TFTs under NBIS. At room temperature, after 15 minutes of fluorine treatment, ΔV_{ON} decreases from 5.53 V to 2.02 V. This improvement is mainly attributed to the fact that fluorine atoms fill the ionized oxygen vacancies in a-IGZO, thereby reducing the density of defect states in the channel. Further adding 2.0 μm wide metal-covered wires reduces the ΔV_{ON} to 0.35 V. Under 80 °C NBIS, the ΔV_{ON} is limited to 3.79 V. This improvement is mainly attributed to the light-shielding effect of the metal lines and the passivation of oxygen vacancies by fluorine, thereby enhancing device stability under NBIS.

Keywords: thin-film transistor (TFT), a-IGZO, negative bias illumination stress (NBIS), stability, fluorination

PACS: 81.05.Gc, 85.30.Tv, 85.30.De

DOI: 10.1088/1674-1056/ae40da **CSTR:** 32038.14.CPB.ae40da

1. Introduction

Amorphous indium gallium zinc oxide (a-IGZO) thin-film transistors (TFTs) have had a significant impact in the field of active-matrix flat-panel displays. This is attributed to the amorphous nature of the active layer and a field-effect mobility exceeding 10 $cm^2 \cdot V^{-1} \cdot s^{-1}$, combined with advantages such as low off-state current, simple fabrication process, and good uniformity.[1] These devices are primarily fabricated using either the back-channel etch (BCE) or the etch-stop layer (ESL) structure. However, the BCE method may cause damage to the back channel during the etching of the source/drain structures, while the ESL approach complicates the manufacturing process.[2–6] Against this backdrop, the elevated metal metal-oxide (EMMO) TFT addresses the issues mentioned above by elevating the metal source/drain electrodes above the passivation layer and forming conductive source/drain regions beneath the corresponding electrodes after annealing.[7]

Light exposure and increased temperature are unavoidable conditions in active-matrix flat-panel displays. Under negative bias illumination stress (NBIS), a continuous negative shift in the transfer characteristics of a-IGZO TFTs can be observed. When the operating temperature increases, the negative shift in the transfer characteristics of a-IGZO TFTs after NBIS becomes more pronounced. Currently, annealing the devices in an oxygen atmosphere can achieve relatively good passivation of oxygen vacancy defects; however, significant device degradation can still be observed under NBIS.[8]

Simply relying on annealing in an oxygen atmosphere to achieve defect passivation is evidently insufficient. Therefore, this paper proposes fluorine doping of the active layer in EMMO TFTs via CF_4 plasma treatment, with the fluorine dosage controlled by adjusting the plasma treatment time.[9] Since fluorine atoms can replace oxygen or occupy oxygen vacancies, fluorine doping can reduce the defect state density and increase the carrier concentration, thereby improving the performance of TFTs.[10] Building upon fluorine doping, metal cover lines are introduced to effectively block incident light and reduce the light power density in a-IGZO. The reason for using metal lines instead of a single metal plate is that during heat-treatment processing, a large number of oxygen vacancies may form under the metal light-blocking layer. These oxygen vacancies enhance the electrical conductivity of the channel region and may eventually lead to the loss of the device switching function. The combination of these two methods can significantly enhance device stability. Based on this, NBIS experiments were conducted on EMMO TFTs, demonstrating the effectiveness of combining fluorine doping with metal cover lines in suppressing device degradation under NBIS.

2. Experiments

The device parameters of the EMMO TFTs used in the experiment are as follows. The structure includes a 300 nm molybdenum (Mo) gate electrode and a gate dielectric stack

†Corresponding author. E-mail: dongli_zhang@suda.edu.cn

© 2026 Chinese Physical Society and IOP Publishing Ltd. All rights, including for text and data mining, AI training, and similar technologies, are reserved.

composed of 75 nm silicon nitride (Si_3N_4) and 125 nm silicon dioxide (SiO_2). The channel active layer of the EMMO TFT is made of 20 nm a-IGZO. After the deposition of the active layer, fluorine doping was performed on the a-IGZO film for some samples using CF_4 plasma treatment, with the fluorine dosage controlled by adjusting the plasma treatment time. In this study, based on the different fluorine treatment durations, samples treated for 0 minute, 5 minutes, 10 minutes, and 15 minutes are labeled as F0-TFT, F5-TFT, F10-TFT, and F15-TFT, respectively. After fluorine treatment, a 300 nm SiO_2 layer was deposited as the passivation layer. Following the deposition of both the gate dielectric and passivation layers, a separate dehydrogenation annealing step was carried out at 400 °C in an oxygen atmosphere for 2 hours to mitigate the potential impact of hydrogen on device performance. For EMMO TFTs without metal cover lines (referred to as W-TFTs), the source/drain metal electrodes are formed using 35 nm Mo and 300 nm aluminum (Al). Additionally, EMMO TFTs with segmented metal cover lines of 2.0 μm width, fabricated simultaneously above the channel passivation layer along with the source/drain electrodes, are referred to as M-TFTs. Figure 1 presents the plane-view optical micrographs of W- and M-TFTs. After annealing at 400 °C in an oxygen atmosphere for 3.5 hours, conductive source and drain regions were formed self-aligned beneath the respective electrodes due to the good sealing property of the source/drain metal electrodes.[11] Figure 2 shows the cross-sectional diagrams and the corresponding simplified process flow of the W-TFTs and M-TFTs.

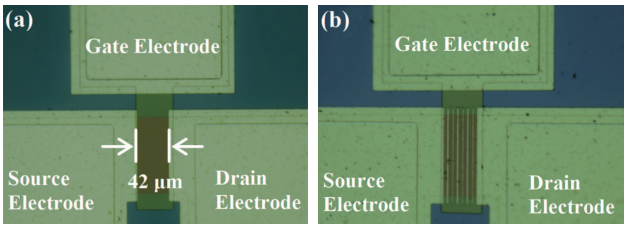


Fig. 1. Optical micrographs of (a) W-TFTs and (b) M-TFTs.

The apparent channel width and length of the devices used in the experiment are 100 μm and 42 μm, respectively. For M-TFTs, the metal line width is 2.0 μm, the spacing between adjacent metal lines is 4.2 μm, and the total coverage of the metal lines over the channel length is 28.99%. The stability experiments are divided into three main groups: (1) NBIS testing at room temperature of 24 °C on W-TFTs with different fluorination times, referred to as W-F0 TFT, W-F5 TFT, W-F10 TFT, and W-F15 TFT; (2) NBIS testing at room temperature on M-TFTs without fluorination (referred to as M-F0 TFT) and with a 15-minute fluorination treatment (referred to as M-F15 TFT); (3) NBIS testing at 40 °C and 80 °C for W-F0, W-F15, M-F0, and M-F15 TFTs. The electrical characteristics of the devices were measured using an Agilent 4156C semiconductor parameter analyzer. The NBIS test conditions were as follows: a gate voltage of −20 V, 445 nm illumination with an intensity of 5.9 mW·cm^{-2}, and a stress duration of 5000 s.

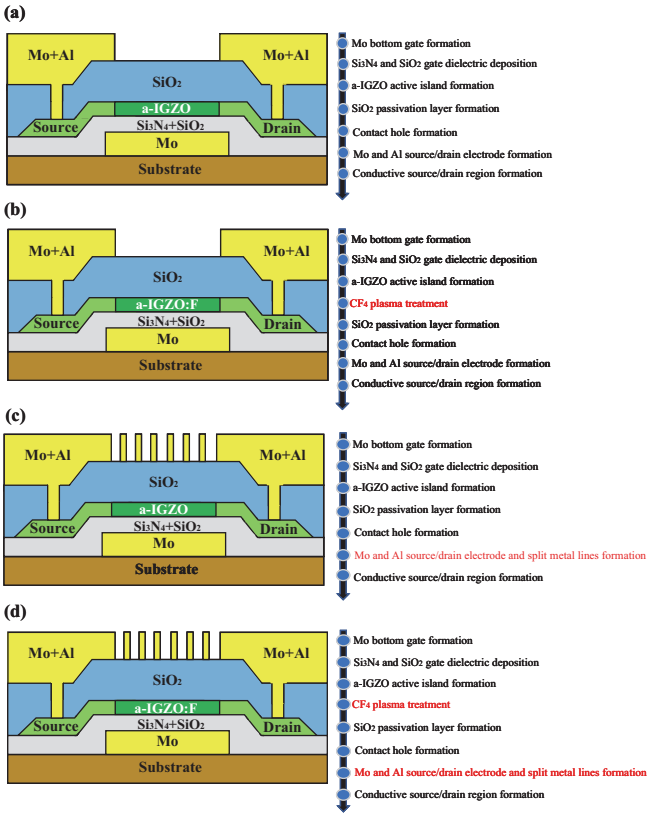


Fig. 2. Cross-sectional diagrams and the corresponding simplified process flow of (a) W-F0 TFT, (b) W-F15 TFT, (c) M-F0 TFT, and (d) M-F15 TFT.

3. Results and discussions

The evolution of the transfer characteristics of W-TFTs under NBIS is shown in Fig. 3. It can be observed that as the fluorine incorporation time increases, the device degradation gradually decreases, with the minimum degradation occurring at 15 minutes of fluorine incorporation. As shown in Fig. 4, the turn-on voltages (V_{ON}) for the pristine W-F0, W-F5, W-F10, and W-F15 TFTs are 0.2 V, 0.2 V, 0.3 V, and 0.3 V, respectively, and the corresponding V_{ON} degradations (ΔV_{ON}) after 5000 s stress are 5.53 V, 4.48 V, 3.07 V, and 2.02 V. The threshold voltages (V_{TH}) extracted from the linear region for the pristine TFTs are 6.6 V, 5.6 V, 6.2 V, and 7.8 V, respectively, and the corresponding V_{TH} degradations (ΔV_{TH}) are 2.83 V, 2.75 V, 1.87 V, and 0.84 V after 5000 s stress.

The data demonstrate that all EMMO TFTs exhibit negative shifts in the transfer characteristics under NBIS, regardless of the fluorination treatment duration. However, with increasing fluorination treatment time, both ΔV_{ON} and ΔV_{TH} show a substantial reduction after 15-minute treatment compared with the untreated device. This improvement is attributed to the passivation of oxygen vacancy defects in the a-IGZO film by fluorine atoms. Since NBIS results from the combined effects of negative gate bias and illumination stress,

fluorine doping in the a-IGZO layer leads to the passivation and reduction of oxygen vacancy defects in the active layer. Consequently, the number of ionized oxygen vacancy defects induced by NBIS that contribute to device degradation decreases, resulting in a reduced negative shift of the transfer curve.[12]

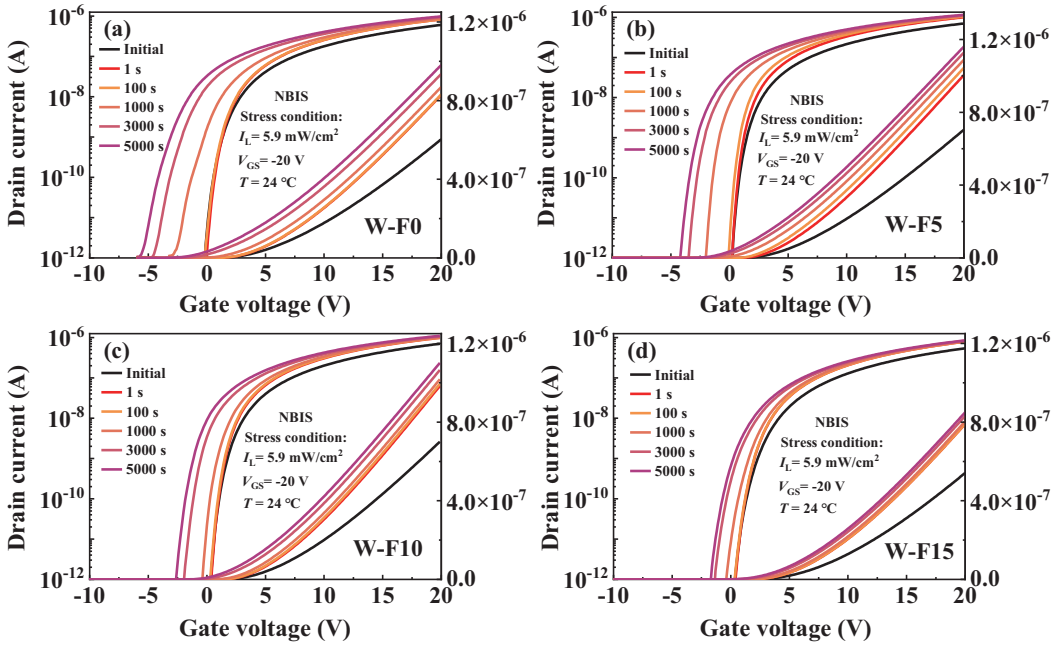


Fig. 3. Evolution of the transfer curves for (a) W-F0, (b) W-F5, (c) W-F10, and (d) W-F15 under NBIS at 24 °C.

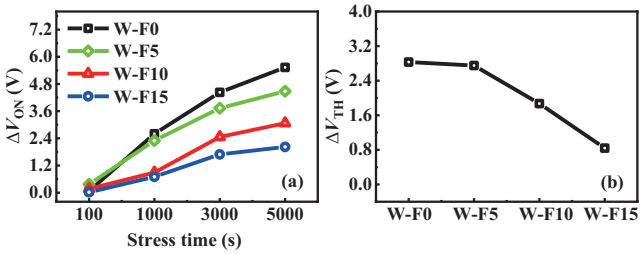


Fig. 4. (a) Comparison of ΔV_{ON} at different stress times and (b) ΔV_{TH} after 5000 s stress for different W-TFTs under NBIS at 24 °C.

In a-IGZO, oxygen-related defects represent a significant class of intrinsic defects. They act as acceptor-like and donor-like trap states and can exist in different forms, i.e., interstitial oxygen, neutral, singly ionized, and doubly ionized oxygen vacancies. The energy levels of neutral oxygen vacancies lie near the valence band maximum. Given that the bandgap of a-IGZO thin films is 3.2 eV, ionizing neutral oxygen vacancies into charged V_O^+ or V_O^{2+} states requires at least 2.3 eV or more.[13,14] Therefore, under blue light illumination with a photon energy of approximately 2.7 eV in our experiments, the conditions are sufficient to ionize neutral oxygen vacancies and contribute free electrons to the conduction band of a-IGZO.[15,16] The energy levels of the ionized oxygen vacancies are located near the conduction band edge (E_C) and are typically described using Gaussian or exponential distributions representing donor-like defect states.

In this work, Silvaco Atlas was employed to fit the experimental transfer characteristics of W-F0, W-F5, W-F10, and W-F15 TFTs, both initially and after 5000 s NBIS. The specific defect density parameters are listed in Table 1. To accurately simulate the transfer characteristics in both the subthreshold and above-threshold regions, Gaussian distributions were selected to model the donor-like defect states within the bandgap. Specifically, oxygen vacancies (V_O^{2+}) with a Gaussian peak located at 3.0 eV relative to the valence band edge (E_V) were used to represent doubly charged oxygen vacancies, while those at 2.7 eV from E_V were used to represent singly charged oxygen vacancies (V_O^+). Figure 5 shows the fitting results between the experimental and simulated transfer characteristics of the initial TFTs and those after 5000 s NBIS. The good agreement between the experimental and simulated curves further confirms the influence of defect states at 3.0 eV and 2.7 eV on the transfer characteristics, supporting the conclusion that oxygen vacancy defects are generated in a-IGZO under bias–illumination stress.

As shown in Fig. 6, the initial density of Gaussian-distributed donor-like defect states gradually decreases with increasing fluorine treatment time. The reduction in these trap states indicates a lower concentration of ionizable oxygen vacancies. Consequently, as fluorine incorporation time increases, the generation of V_O^+ and V_O^{2+} via ionization is suppressed. The W-F15 TFT with the longest fluorine treatment time exhibits the least degradation in transfer characteristics because of the lowest defect state density due to passivation of oxygen vacancies and the strongest capability to suppress NBIS-induced degradation.[17–19] After 5000 s of stress, it is also evident that the sample with 15 minutes of fluorine in-

corporation exhibits the smallest increase in N_{GD}, resulting in minimal device degradation. Although a 15 minute fluorination treatment exhibits the most effective suppression of NBIS, an evaluation of the overall device performance reveals that increasing the doping duration from 10 minutes to 15 minutes leads to a reduction in the on-state current and an increase in the acceptor-like trap states near the conduction band. Consequently, considering both stability and electrical performance, a fluorine doping duration of 15 minutes is determined to be the optimal condition.

Table 1. Parameters for the trap states in the a-IGZO of W-TFTs before and after 5000 s NBIS.

Value / Parameter	a-IGZO:F0		a-IGZO:F5		a-IGZO:F10		a-IGZO:F15	
	Initial	NBIS	Initial	NBIS	Initial	NBIS	Initial	NBIS
N_{TA} ($\times10^{18}$) ($cm^{-3}eV^{-1}$)	7.0	7.0	7.4	7.4	7.8	9.5	8.2	8.0
W_{TA} (eV)	0.105	0.105	0.105	0.105	0.105	0.105	0.105	0.105
N_{TD} ($\times10^{20}$) ($cm^{-3}eV^{-1}$)	8.0	8.0	8.0	8.0	8.0	8.0	8.0	8.0
W_{TD} (eV)	0.1	0.1	0.1	0.1	0.1	0.1	0.1	0.1
N_{GA} ($\times10^{17}$) ($cm^{-3}eV^{-1}$)	5.5	5.5	5.6	5.6	5.9	5.9	6.0	6.0
E_{GA} (eV)	1.0	1.0	1.0	1.0	1.0	1.0	1.0	1.0
W_{GA} (eV)	0.1	0.1	0.1	0.1	0.1	0.1	0.1	0.1
N_{GD1} ($\times10^{18}$) ($cm^{-3}eV^{-1}$)	0.33	6.3	0.15	5.2	0.11	2.4	0.1	1.1
E_{GD1} (eV)	3.0	3.0	3.0	3.0	3.0	3.0	3.0	3.0
W_{GD1} (eV)	0.1	0.1	0.1	0.1	0.1	0.1	0.1	0.1
N_{GD2} ($\times10^{18}$) ($cm^{-3}eV^{-1}$)	0.2	3.5	0.15	1.5	0.11	0.6	0.1	0.2
E_{GD2} (eV)	2.7	2.7	2.7	2.7	2.7	2.7	2.7	2.7
W_{GD2} (eV)	0.1	0.1	0.1	0.1	0.1	0.1	0.1	0.1

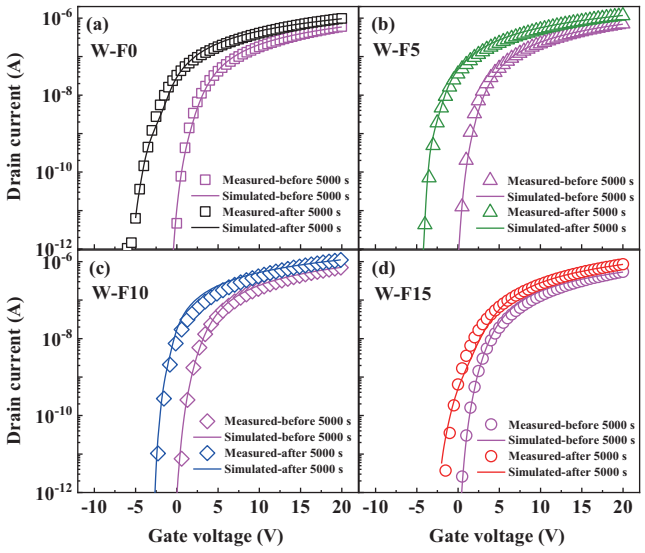


Fig. 5. Fitting results for the transfer curves of (a) W-F0, (b) W-F5, (c) W-F10, and (d) W-F15 TFTs before and after 5000 s NBIS.

For the M-TFTs, the metal cover lines function to block incident light and reduce the light power density absorbed by the a-IGZO thin film.[20] Therefore, as shown in Fig. 7, the transfer characteristics of M-F0 and M-F15 TFTs under NBIS at 24 °C exhibit much reduced degradation. One can notice in Fig. 8 that ΔV_{ON} is 0.35 V for M-F15 TFT and 1.68 V for M-F0 TFT after 5000 s stress. This demonstrates that the advantage brought by fluorine doping remains evident. Furthermore, compared to the degradation of W-F0 TFTs without metal cover lines, the metal cover line structure also demonstrates a clear effect in suppressing degradation. In conclusion, both fluorine incorporation and the metal cover line structure effectively inhibit NBIS-induced degradation and enhance device reliability. Their combination provides better NBIS suppression effects.

At room temperature, superior reliability of the device under NBIS was achieved with the incorporation of fluorine passivation and illumination-shielding metal lines. NBIS degradation is temperature-activated; therefore, the experimental substrate temperature was increased to 40 °C and 80 °C to evaluate the effectiveness of fluorine passivation and illumination shielding on the suppression of NBIS degradation. As shown in Fig. 8, at 24 °C, the ΔV_{ON} gradually decreases with

increasing fluorination treatment time. After 15 minutes of fluorination treatment, ΔV_{ON} decreases from 5.53 V to 2.02 V, representing a 63.5 % reduction in degradation. Since the introduction of fluorine does not affect the reflection, refraction, or absorption of light in the TFT, its primary role is to reduce the neutral oxygen vacancy density, thereby decreasing the amount of newly ionized oxygen vacancies and consequently reducing the impact on the TFT's transfer characteristics. When the metal line width is 2.0 μm, ΔV_{ON} is reduced from 5.53 V to 1.68 V, a 69.6 % reduction. This indicates that the light-blocking effect of metal lines provides slightly better NBIS inhibition than fluorine passivation. The better NBIS inhibition effect of light-blocking becomes more obvious at the higher stress temperatures of 40 °C and 80 °C. However, as shown in Fig. 9, the effects of fluorination and metal line light-blocking on NBIS degradation inhibition both become less pronounced at higher temperatures.

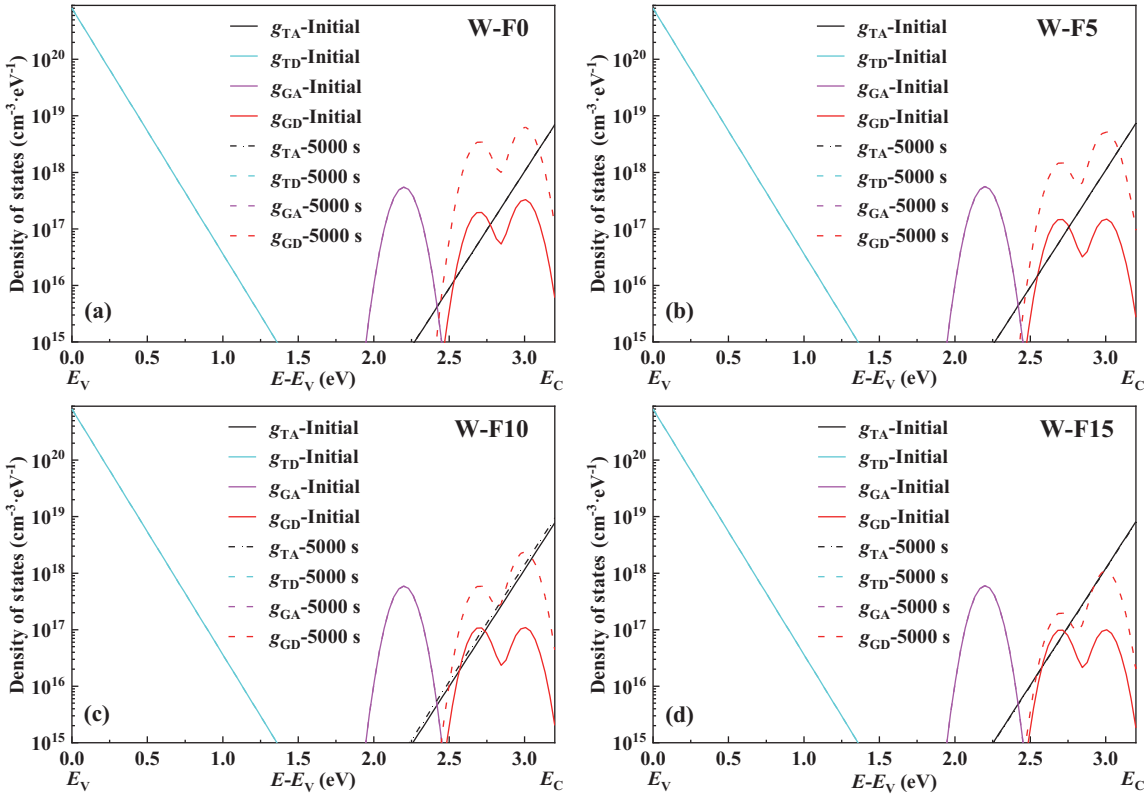


Fig. 6. Distribution of the trap states in the channel a-IGZO in (a) W-F0 TFT, (b) W-F5 TFT, (c) W-F10 TFT, and (d) W-F15 TFT before and after 5000 s NBIS.

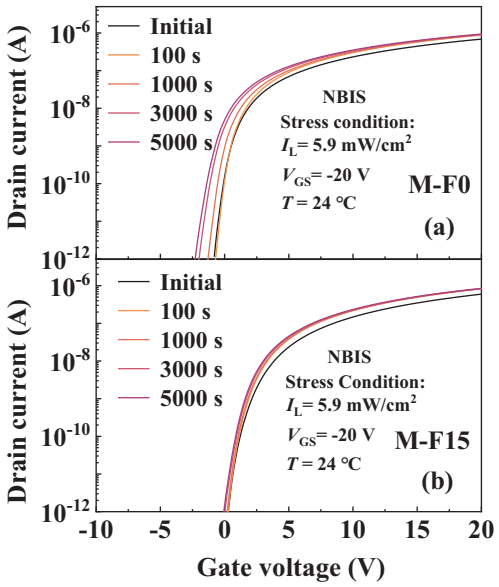


Fig. 7. Evolutions of the transfer curves of (a) M-F0 TFT and (b) M-F15 TFT under NBIS at 24 °C.

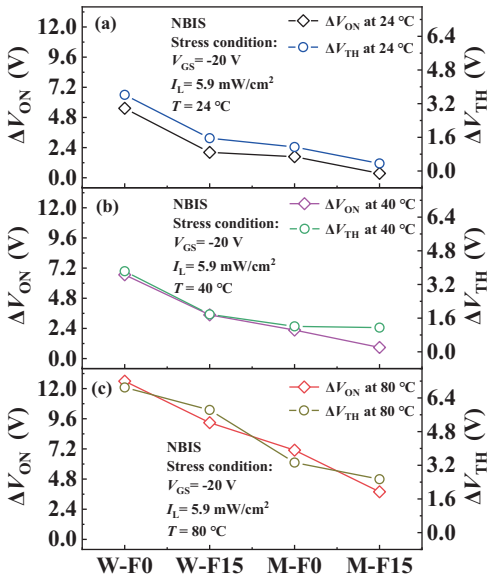


Fig. 8. ΔV_{ON} and ΔV_{TH} of W-F0, W-F15, M-F0, and M-F15 TFTs after 5000 s NBIS at 24 °C, 40 °C, and 80 °C.

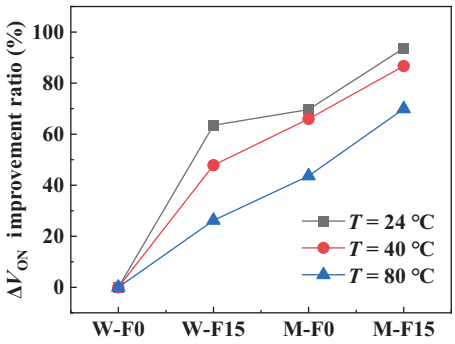


Fig. 9. ΔV_{ON} improvement ratio for W-F15, M-F0, and M-F15 TFTs over W-F0 TFTs at different stress temperatures.

Furthermore, we observed that the combined effect of 15 minutes of fluorination treatment and 2.0 μm metal lines in inhibiting NBIS degradation is not simply additive. The ΔV_{ON} improvement ratio for the TFTs with fluorination for 15 minutes and 2.0 μm metal lines over the TFTs without fluorination treatment and metal lines is derived as the difference between the ΔV_{ON} of TFTs without fluorination/metal lines and that of TFTs with both treatments, divided by the ΔV_{ON} of TFTs without these treatments. At 24 °C, 40 °C, and 80 °C, the ΔV_{ON} improvement ratio reached 93.7 %, 86.7 %, and 69.9 %, respectively. One can thus notice that the a-IGZO TFT with 2.0 μm metal lines and 15 minutes of fluorination exhibits better NBIS stability than those reported in Refs. [21–23].

4. Conclusion

EMMO TFTs with CF_4 plasma treatment demonstrated improved stability under NBIS at room temperature. As the fluorine incorporation time increased to 15 minutes, the ability to suppress instability was the strongest. When fluorine doping was combined with the metal cover line structure, it was found that this combination provided an even greater advantage in mitigating NBIS-induced degradation, outperforming the cases with only fluorine doping or only the metal cover line structure. Fluorine doping reduces the number of defects in the pristine a-IGZO film, while the metal cover line lowers the light power density within the a-IGZO film. Therefore, from the point of view of NBIS suppression, both the oxygen vacancies and light power in the channel a-IGZO should be minimized.

Acknowledgments

Project supported by the National Natural Science Foundation of China (Grant No. 62371327) and the Jiangsu Provincial Key Research and Development Program (Grant No. BE2022058-4).

References

[1] Geng D, Wang K, Li L, Myny K, Nathan A, Jang J, Kuo Y and Liu M 2023 *Nat. Electron.* **6** 963
[2] Zhang G, Xu Y, Haider M, Sun J, Zhang D and Yang J 2023 *Appl. Phys. Rev.* **10** 031313
[3] Park J S, Maeng W J, Kim H S and Park J S 2012 *Thin Solid Films* **520** 1679
[4] Yamazaki S, Hirohashi T, Takahashi M and Matsuo T 2014 *J. Soc. Inf. Disp.* **22** 55
[5] Deng W, Xiao X, Shao Y, Song Z, Lee C Y, Lien A and Zhang S 2016 *IEEE Trans. Electron Devices* **63** 1
[6] Nag M, Steudel S, Bhoolokam A, Chasin A, Rockele M, Myny K, Maas J, Fritz T, Trube J, Groeseneken G and Heremans P 2014 *J. Soc. Inf. Disp.* **22** 23
[7] Lu L, Li J, Feng Z, Kwok H S and Wong M 2016 *IEEE Electron Device Lett.* **37** 728
[8] Lu L and Wong M 2015 *IEEE Trans. Electron Devices* **62** 574
[9] Xia Z, Lu L, Li J and Wong M 2018 *SID Int. Symp. Dig. Tech. Pap.* **49** 1235
[10] Seo J S, Jeon J H, Hwang Y H, Park H, Ryu M, Park S H K and Bae B S 2013 *Sci. Rep.* **3** 2085
[11] Lv N, Lu L, Wang Z, Wang H, Zhang D and Wong M 2020 *IEEE Trans. Electron Devices* **67** 3001
[12] Jiang W, Xia Z and Wong M 2023 *IEEE Trans. Electron Devices* **71** 1084
[13] Kamiya T and Hosono H 2010 *NPG Asia Mater.* **2** 15
[14] Kamiya T, Nomura K, Hirano M and Hosono H 2008 *Phys. Status Solidi C* **5** 3098
[15] Ji K H, Kim J I, Jung H Y, Park S Y, Choi R, Mo Y G and Jeong J K 2011 *Microelectron. Eng.* **88** 1412
[16] Furuta M, Hung M P, Jiang J, Wang D, Tomai S, Hayasaka H and Yano K 2013 *ECS Trans.* **54** 127
[17] Chen P C, Chiu Y C, Zheng Z W, Cheng C H and Wu Y H 2017 *J. Alloys Compd.* **707** 162
[18] Zhang Y Y, Qian L X, Lai P T, Dai T J and Liu X Z 2019 *IEEE Electron Device Lett.* **40** 1646
[19] Sio H C, Kang D, Samundsett C and Macdonald D 2021 *IEEE 48th Photovoltaic Specialists Conference (PVSC)* pp. 0729
[20] Feng Y, Lv N, Zhang D, Wang H, Lu L, Wong M and Wang M 2025 *IEEE J. Electron Devices Soc.* **13** 1075
[21] Tu Y F, Lu I N, Chen H C, Su W C, Hung Y H, Zhou K J, Zheng Y Z, Sun L C, Shih Y S, Chen J J, Lien C Y, Huang H C and Lien C H 2020 *IEEE Electron Device Lett.* **41** 1221
[22] Lee S, Mativenga M and Jang J 2014 *IEEE Electron Device Lett.* **35** 930
[23] Bian L, Wu J, Shen Y, He S, Xue S, Zhang M and Yan Y 2025 *IEEE International Conference on Electron Devices and Solid-State Circuits (EDSS)* pp. 46